AKAP79/150 recruits the transcription factor NFAT to regulate signaling to the nucleus by neuronal L-type Ca^{2+} channels

Jonathan G. Murphy[a,b,†], Kevin C. Crosby[b,†], Philip J. Dittmer[b], William A. Sather[b], and Mark L. Dell'Acqua[b,*]

[a]Eunice Kennedy Shriver Institute for Child Health and Human Development, National Institutes of Health, Bethesda, MD 20892; [b]Department of Pharmacology, University of Colorado School of Medicine, Aurora, CO 80045

ABSTRACT **In neurons, regulation of activity-dependent transcription by the nuclear factor of activated T-cells (NFAT) depends upon Ca^{2+} influx through voltage-gated L-type calcium channels (LTCC) and NFAT translocation to the nucleus following its dephosphorylation by the Ca^{2+}-dependent phosphatase calcineurin (CaN). CaN is recruited to the channel by A-kinase anchoring protein (AKAP) 79/150, which binds to the LTCC C-terminus via a modified leucine-zipper (LZ) interaction. Here we sought to gain new insights into how LTCCs and signaling to NFAT are regulated by this LZ interaction. RNA interference–mediated knockdown of endogenous AKAP150 and replacement with human AKAP79 lacking its C-terminal LZ domain resulted in loss of depolarization-stimulated NFAT signaling in rat hippocampal neurons. However, the LZ mutation had little impact on the AKAP–LTCC interaction or LTCC function, as measured by Förster resonance energy transfer, Ca^{2+} imaging, and electrophysiological recordings. AKAP79 and NFAT coimmunoprecipitated when coexpressed in heterologous cells, and the LZ mutation disrupted this association. Critically, measurements of NFAT mobility in neurons employing fluorescence recovery after photobleaching and fluorescence correlation spectroscopy provided further evidence for an AKAP79 LZ interaction with NFAT. These findings suggest that the AKAP79/150 LZ motif functions to recruit NFAT to the LTCC signaling complex to promote its activation by AKAP-anchored calcineurin.**

Monitoring Editor
A. Gregory Matera
University of North Carolina

Received: Jan 28, 2019
Revised: May 3, 2019
Accepted: May 7, 2019

INTRODUCTION

The Ca_V1 family of L-type voltage-gated Ca^{2+} channels (LTCCs) are widely expressed and regulate important physiological processes including insulin secretion, muscle contraction, rhythmic firing, neurotransmitter release, and transcription (Catterall, 2011). In neurons, LTCCs both provide depolarizing inward Ca^{2+} current and initiate Ca^{2+}-dependent intracellular signaling cascades. LTCCs are advantaged with respect to other voltage-gated Ca^{2+} channels in activating neuronal gene expression programs in response to electrical excitation (Ma *et al.*, 2013). LTCC-mediated excitation–transcription coupling alters gene expression by downstream signaling to transcription factors, including the cAMP response element–binding protein (CREB) and the nuclear factor of activated T-cells (NFAT; Murphy *et al.*, 1991; Bading *et al.*, 1993; Graef *et al.*, 1999; Dolmetsch *et al.*, 2001). Persistent changes in transcription and protein translation in neurons are required for long-lasting forms of synaptic long-term potentiation (L-LTP), processes that alter neuronal circuit connectivity with a duration that extends from hours to months and is regarded as a key cellular correlate for neuronal memory (Malenka and Bear, 2004). The NMDA receptor-independent form of L-LTP requires LTCCs, as demonstrated by blockade of channel function using dihydropyridine antagonists and in $Ca_V1.2$ knockout animals (Grover and Teyler, 1990; Grover, 1998; Morgan and Teyler, 1999). For example, mice with conditional knockout of

This article was published online ahead of print in MBoC in Press (http://www.molbiolcell.org/cgi/doi/10.1091/mbc.E19-01-0060) on May 15, 2019.

†These authors contributed equally to this work.

The authors declare no competing financial interests.

*Address correspondence to: Mark L. Dell'Acqua (mark.dellacqua@ucdenver.edu).

Abbreviations used: AKAP79/150, A-kinase anchoring protein 79/150; CaN, calcineurin, a.k.a. protein phosphatase 3; CDI, Ca^{2+}-dependent inactivation; FCS, fluorescence correlation spectroscopy; FRAP, fluorescence recovery after photobleaching; FRET, Förster resonance energy transfer; LTCC, L-type Ca^{2+} channel; LZ, leucine zipper; NFAT, nuclear factor of activated T-cells; TTX, tetrodotoxin.

the predominant LTCC isoform in the forebrain, $Ca_V1.2$, have reduced NMDA receptor-independent L-LTP, spatial learning, and CREB activation (Moosmang *et al.*, 2005). The importance of $Ca_V1.2$ in synaptic plasticity and brain function, not only in mice but also in humans, is evident from the link between alterations in channel function and polymorphisms of the human *CACNA1C* gene found in multiple neuropsychiatric disorders including Parkinson's disease, Alzheimer's disease, schizophrenia, and autism-spectrum disorders (Ortner and Striessnig, 2016). Therefore, a better understanding of the mechanisms that control LTCC function in neurons, especially with regard to excitation–transcription signaling, is critical to our understanding of cognition and brain function.

A-kinase anchoring protein (AKAP) 79/150 (human 79/rodent 150; also known as AKAP5) is a multidomain scaffolding protein that imparts spatial specificity and temporal precision to intracellular signaling by anchoring kinases, phosphatases, and components of the cAMP signaling pathway, including adenylyl cyclases and phosphodiesterases, to plasma membrane structures (Dell'Acqua *et al.*, 1998; Bauman *et al.*, 2006; Efendiev *et al.*, 2010; Woolfrey and Dell'Acqua, 2015). In neurons, AKAP79/150 is an indispensable component of the postsynaptic proteome that regulates the phosphorylation state of postsynaptic glutamate receptors and ion channels (reviewed in Wild and Dell'Acqua, 2018) through recruitment of cAMP-dependent protein kinase (PKA), protein kinase C (PKC), and the protein phosphatase calcineurin (CaN; also known as PP2B and PPP3; Carr *et al.*, 1992; Coghlan *et al.*, 1995; Klauck *et al.*, 1996; Tavalin, 2008). In particular, AKAP79/150 interacts directly with LTCCs and bidirectionally regulates channel phosphorylation and function through local anchoring of PKA and CaN (Gao *et al.*, 1997; Oliveria *et al.*, 2007, 2012; Dittmer *et al.*, 2014; Murphy *et al.*, 2014). The activity of enzymes anchored within this multiprotein complex determines the shape and size of the Ca^{2+} signal that is generated by the channel. Basal-channel phosphorylation and activity are maintained by AKAP79/150–targeted PKA (Dittmer *et al.*, 2014; Murphy *et al.*, 2014), while AKAP79/150 targeting of CaN limits basal phosphorylation and activity and also imparts negative feedback regulation of the amount and duration of Ca^{2+} entry in a process known as Ca^{2+}-dependent inactivation (CDI; Peterson *et al.*, 1999; Erickson *et al.*, 2001; Oliveria *et al.*, 2012).

In addition to the important role of AKAP79/150 in regulating LTCC channel function, dynamic AKAP anchoring of CaN is required for NFAT signaling (Li *et al.*, 2012). When bound to the C-terminus of LTCCs, the Ca^{2+} sensor calmodulin (CaM) responds to channel Ca^{2+} entry to activate AKAP79/150–anchored CaN (Oliveria *et al.*, 2012). Upon Ca^{2+}/CaM-dependent CaN activation and dissociation from the nonconsensus PxIxIT-motif of AKAP79/150, CaN dephosphorylates NFAT, exposing a nuclear localization signal that results in nuclear import (Beals *et al.*, 1997; Li *et al.*, 2012). The AKAP79/150 complex associates with the LTCC at least in part through a predicted coiled-coil interaction of C terminal–modified leucine zipper motifs (LZ) located between residues 408-427 of human AKAP79 (695-714 of rat orthologue AKAP150) and 2072-2102 of human $Ca_V1.2$. We previously demonstrated that point mutations introduced simultaneously into the LZ domains of both AKAP79 and $Ca_V1.2$ disrupted the AKAP–$Ca_V1.2$ interaction, resulting in a loss of PKA/CaN regulation of $Ca_V1.2$ through AKAP uncoupling from the channel (Oliveria *et al.*, 2007).

In this study, we present new information regarding the importance of the AKAP79/150 LZ motif in regulation of NFAT-based excitation–transcription signaling. In particular, we show that the AKAP79/150 LZ motif likely functions to recruit NFAT to the AKAP–LTCC complex at the plasma membrane to promote its activation by Ca^{2+}–CaN signaling.

RESULTS

The AKAP LZ motif regulates depolarization-triggered NFAT translocation and transcription in cultured hippocampal neurons

In hippocampal neurons, LTCC Ca^{2+} entry activates CaN-mediated NFAT translocation and transcription in the nucleus (Graef *et al.*, 1999; Oliveria *et al.*, 2007; Murphy *et al.*, 2014). We previously established that complementary modified LZ motifs on AKAP and the LTCC promote formation of the AKAP–LTCC complex. To study a potential role for the AKAP79/150 LZ motif in NFAT signaling, we generated a 17–amino acid carboxyl-terminal (C-terminal) truncation of AKAP79, creating a 410–amino acid AKAP79 fragment (Figure 1A). This AKAP79 LZ motif deletion (ΔLZ) eliminates two of the three critical heptad spaced hydrophobic residues that form the modified LZ, while retaining the adjacent portion of the amphipathic α-helical motif that is required for PKA anchoring. To determine whether the AKAP LZ is required for NFAT translocation, we first transfected rat hippocampal neurons cultured for 12–14 d in vitro (DIV) with a control pSilencer short-hairpin RNA (shRNA) vector, GFP–NFATc3, and mCherry (mCh). Because spontaneous activity in neuronal cultures is known to drive NFAT signaling (Graef *et al.*, 1999; Murphy *et al.*, 2014), neurons were preincubated with the voltage-gated sodium channel blocker tetrodotoxin (TTX; 1 μM) for 1 h to block spontaneous action potential firing and to allow nuclear export of GFP–NFATc3 to achieve a baseline nonstimulated state. After TTX preincubation, an exchange from 5 mM K^+ to an isotonic 50 mM K^+ Tyrode's solution for 3 min was used to depolarize the neurons and activate LTCC-dependent excitation–transcription coupling. High K^+ depolarization triggered translocation of GFP–NFATc3 into the nucleus, which returned to the cytoplasm after 30 min. GFP–NFATc3 nuclear immunofluorescence peaked at 10 min poststimulation with >7-fold increase in the nucleus-to-cytoplasm ratio from that in nonstimulated neurons (Figure 1, B and C). After shRNA-mediated knockdown of AKAP150, GFP–NFATc3 translocation was significantly reduced (Figure 1, B and C). Human AKAP79 and rat AKAP150 are highly conserved functional homologues that differ only by insertion of a repeat region of unknown significance found in the rodent isoforms, but not in those of any other species. The 150 shRNA targets this rodent-specific repeat region, allowing rescue with the inherently RNA interference (RNAi)-insensitive human version that lacks this repeat region in a well-established knockdown/replacement strategy used by our laboratory and others (Hoshi *et al.*, 2005; Oliveria *et al.*, 2007). Importantly, coexpression of RNAi-resistant human AKAP79ΔLZ-mCh with AKAP150 shRNA could not rescue the deficit in GFP–NFATc3 translocation, while AKAP79WT–mCh restored NFAT translocation.

In our previous work, we showed that NFAT nuclear translocation is correlated with NFAT-dependent transcription (Li *et al.*, 2012; Murphy *et al.*, 2014). To examine whether the AKAP79 LZ regulates NFAT-dependent transcription, we coexpressed either pSilencer control or AKAP150 shRNA plasmid with YFP, AKAP79WT–YFP, or AKAP79ΔLZ–YFP in the presence of a previously described CFP-based NFAT-dependent transcriptional reporter (Li *et al.*, 2012). After a 16-h preincubation in 1 μM TTX to achieve a uniform baseline of NFAT transcriptional activity, neurons were depolarized for 3 min with 90 mM K^+ and fixed 16 h after stimulation. An ~1.5-fold increase in transcription reporter signal was detected in control rat neurons relative to nonstimulated controls (Figure 1, D and E). Consistent with results from NFAT translocation experiments, AKAP150 RNAi abolished stimulation of NFAT-dependent transcription and

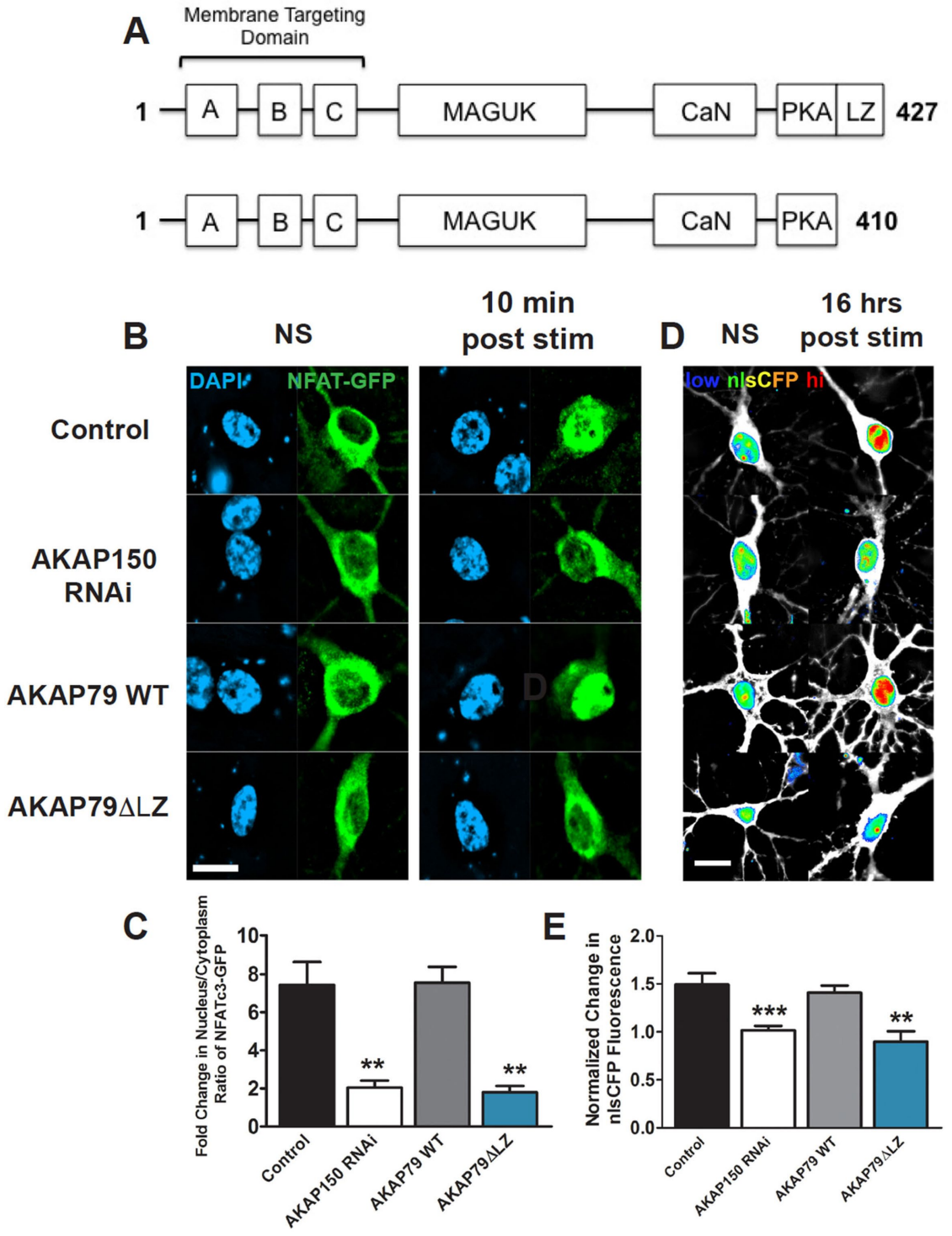

FIGURE 1: The AKAP79/150 LZ motif is required for depolarization-triggered NFATc3 signaling to the nucleus. (A) AKAP79 domain schematic. (B) Summed–intensity projection images of GFP–NFATc3 (green) and nuclei (DAPI, blue) in rat hippocampal neurons transfected with pSilencer empty vector (control) or AKAP150 shRNA plus mCherry (mCh) alone, AKAP79–mCh WT, ΔLZ (mCh images not shown) under nonstimulated (NS) conditions and 10 min after high K^+ stimulation. (C) Quantification of GFP–NFATc3 translocation to nucleus 10 min after high K^+ stimulation measured as the fold change in GFP fluorescence nucleus/cytoplasm ratio relative to NS conditions. (D) Summed–intensity projection images of neuronal cell bodies and proximal dendrites in NS conditions and 16 h after high K^+ stimulation (KCl). Neurons were transfected with the 3xNFAT/AP1-CFPnls reporter along with pSilencer empty vector (control) or AKAP150 shRNA plus YFP or the indicated AKAP79–YFP constructs. YFP fluorescence is in white and nuclear-localized CFP fluorescence is in pseudocolor. (E) Quantification of the fold change in nuclear fluorescence of the 3xNFAT/AP1-CFPnls reporter following high K^+ stimulation for the indicated conditions. Data expressed as mean ± SEM (***$p < 0.001$,**$p < 0.01$; ANOVA with Dunnett's post hoc test; n [translocation assay] = 6–16; n [transcription assay] = 14–49). Scale bar = 10 μm.

expression of AKAP79WT rescued transcription, while AKAP79ΔLZ did not (Figure 1, D and E). These results provide strong evidence supporting a requirement for the AKAP LZ motif in neuronal NFAT signaling.

The AKAP79 LZ motif modestly regulates depolarization-triggered Ca^{2+} dynamics in spines, dendrites, and somata

NFATc3 nuclear signaling is dependent upon LTCC-mediated Ca^{2+} entry; therefore we wanted to determine whether AKAP79 LZ deletion had any effect on Ca^{2+} signals initiated by LTCC opening. To measure changes in intracellular Ca^{2+}, we expressed the genetically encoded Ca^{2+} sensor GCaMP6f in cultured hippocampal neurons. We also expressed either WT or ΔLZ mutant AKAP79-mCh, both as a fluorescent marker to visualize cellular morphology and to further characterize the function of the LZ domain in LTCC-dependent Ca^{2+} signaling. For these experiments, all neurons also expressed the AKAP150 shRNA vector; we previously reported that AKAP150 shRNA strongly reduces LTCC Ca^{2+} signals in neurons, but coexpression of AKAP79WT–mCh rescues these Ca^{2+} signals (as detected by GCaMP6f) to match control (pSilencer) levels (Murphy *et al.*, 2014). For each neuron, a depolarization-induced Ca^{2+} transient was triggered by rapid bath exchange with 90 mM K^+ for 15 s with images captured at 1 Hz throughout the protocol (Figure 2A). In neurons expressing AKAP79WT (Figure 2, B and D, top), K^+ depolarization triggered a large Ca^{2+} signal in spines, dendrites, and the neuronal soma with rapid onset and prolonged resolution lasting several seconds after high K^+ washout (Figure 2, B and C, black traces). The LTCC contribution to the GCaMP6f Ca^{2+} signal was separated from those mediated by other Ca^{2+} channels by addition of the dihydropyridine LTCC antagonist nimodipine (10 μM) during a second depolarization (Figure 2C, red traces). Because both the duration and amplitude of the Ca^{2+} signal were reduced by nimodipine block, we compared the integral of the Ca^{2+} response across conditions and neuronal subcompartments (Figure 2C). In neurons expressing either AKAP79WT or AKAP79ΔLZ, we observed a significant reduction in the GCaMP6f signal in all neuronal subcompartments in the presence of nimodipine (Figure 2C). However, comparison of the LTCC fraction $\left(1-\left(\left(\frac{\int \Delta F_{nim}}{\int \Delta F_{veh}}\right)/F_0\right)\right)$ of the total GCaMP6f response to K^+ depolarization revealed that, in comparison with AKAP79WT, AKAP79ΔLZ-expressing neurons exhibited somewhat reduced LTCC contributions to Ca^{2+} response in spines (WT 0.54 ± 0.3; ΔLZ 0.38 ± 0.6), dendrites (WT 0.65 ± 0.6; ΔLZ 0.50 ± 0.6), and somata (WT 0.77 ± 0.3; ΔLZ 0.59 ± 0.6; Figure 2F). These data indicate that LTCC contributions to Ca^{2+} signals in spines, dendrites, and somata of hippocampal neurons are modestly (~15%) impacted by deletion of the AKAP LZ domain.

Deletion of the AKAP LZ motif alters but does not completely disrupt association with LTCCs

NFAT signaling is initiated by LTCC Ca^{2+} entry and positioning of CaN within the LTCC nanodomain by AKAP79/150 (Graef *et al.*, 1999; Oliveria *et al.*, 2003, 2007; Li *et al.*, 2012); therefore, loss of NFAT signaling could arise due to disruption of the AKAP–LTCC complex by the AKAP79ΔLZ mutation. We sought to determine whether the AKAP79ΔLZ deletion alone affects the formation of the AKAP-LTCC complex using Förster resonance energy transfer (FRET), a method we have previously used to characterize the interaction of AKAP79 and $Ca_V1.2$ LZ (Oliveria *et al.*, 2007; Li *et al.*, 2012; Murphy *et al.*, 2014). We expressed the FRET donors AKAP79WT–CFP or AKAP79ΔLZ–CFP and the FRET acceptor $Ca_V1.2$ fused with YFP at either the N or C terminus in tsA-201 cells (Figure 3A). FRET signals were imaged using sensitized corrected three filter–based FRET ($FRET^C$) and quantified as apparent FRET efficiency (E_{eff}; see *Materials and Methods* for more details; Figure 3B). AKAP79WT–CFP and AKAP79ΔLZ–CFP were primarily localized to the plasma membrane, a subcellular distribution consistent with endogenous AKAP79/150 localization in various cell types. Both versions of the $Ca_V1.2$ construct, YFP–$Ca_V1.2$ and $Ca_V1.2$–YFP, displayed a mix between internal and plasma membrane distribution; however, $FRET^C$ signals were detected only at the plasma membrane in regions of AKAP79 expression, providing an important internal control for the specificity of FRET in detecting AKAP–$Ca_V1.2$ complexes assembled at the plasma membrane. When WT AKAP79WT–CFP was coexpressed with either $Ca_V1.2$ construct, FRET was observed (E_{eff}: 10.79 ± 1.70% for YFP–$Ca_V1.2$; 11.49 ± 1.32% $Ca_V1.2$–YFP; Figure 3, A and B). Comparatively, cells expressing AKAP79ΔLZ–CFP along with the C-terminally tagged channel $Ca_V1.2$–YFP showed significantly less FRET (E_{eff}: 4.15 ± 1.21%) than WT; however, FRET levels did not change significantly (E_{eff}: 12.80 ± 2.53%) when AKAP79ΔLZ–CFP was expressed together with the N-terminally tagged channel YFP–$Ca_V1.2$. It is not possible to discern whether deletion of the C-terminal LZ domain of AKAP79 reduced FRET with the C-terminally tagged channel due to reduced AKAP79–LTCC binding or because of FRET acceptor reorientation within the complex. In either case, these results suggest that, while elimination of the AKAP LZ domain may somewhat alter the AKAP79–LTCC interaction at the plasma membrane, it does not completely disrupt this interaction.

The AKAP79 LZ motif is not required for basal PKA/CaN regulation of LTCC currents

Given the results of our FRET and Ca^{2+} imaging experiments showing only modest impacts on the AKAP–LTCC interaction and Ca^{2+} signals, we next sought to evaluate even more directly what impact the AKAP79ΔLZ mutation might have on channel function. In neurons, CDI is tightly regulated by highly localized LTCC Ca^{2+} entry, which is insensitive to intracellular application of high concentrations (10 mM) of the slow Ca^{2+} chelator ethylene glycol-bis(β-aminoethyl ether)-*N*,*N*,*N*′,*N*′-tetraacetic acid (EGTA) and can largely be distinguished from voltage-dependent inactivation by the use of extracellular Ba^{2+} as the charge carrier (Brehm and Eckert, 1978). Our previous work showed that AKAP79/150 recruitment of CaN within the EGTA-insensitive LTCC Ca^{2+} nanodomain is critical for neuronal CDI (Oliveria *et al.*, 2012). In addition, we showed that a mutant AKAP79 lacking the PKA-RII anchoring domain (AKAP79ΔPKA), which reduces depolarization-triggered Ca^{2+} rises like AKAP79ΔLZ (albeit more strongly), also reduces LTCC current density and impairs CDI of neuronal LTCCs, as measured using whole-cell recordings (Dittmer *et al.*, 2014). Here, we measured both CDI and LTCC current density (with 10 mM EGTA intracellular) in neurons expressing AKAP150 shRNA with or without coexpression of AKAP79WT–GFP or AKAP79ΔLZ–GFP.

Under whole-cell voltage clamp, pharmacologically isolated LTCC currents were elicited from rat neurons cultured 3–4 DIV using a 500-ms step depolarization to 0 mV from a holding potential of –60 mV. As expected for WT control rat neurons, depolarization elicited an inward current that exhibited rapid, strong inactivation with Ca^{2+} as the charge-carrying permeant ion (that is, CDI; Figure 3, C–F, middle, red trace), but not when Ca^{2+} was replaced by Ba^{2+} in the bath (Figure 3, C–F, middle, black trace; slow decay remaining in these records represents the voltage-dependent component of inactivation). The Ca^{2+} and Ba^{2+} currents recorded from the same cell

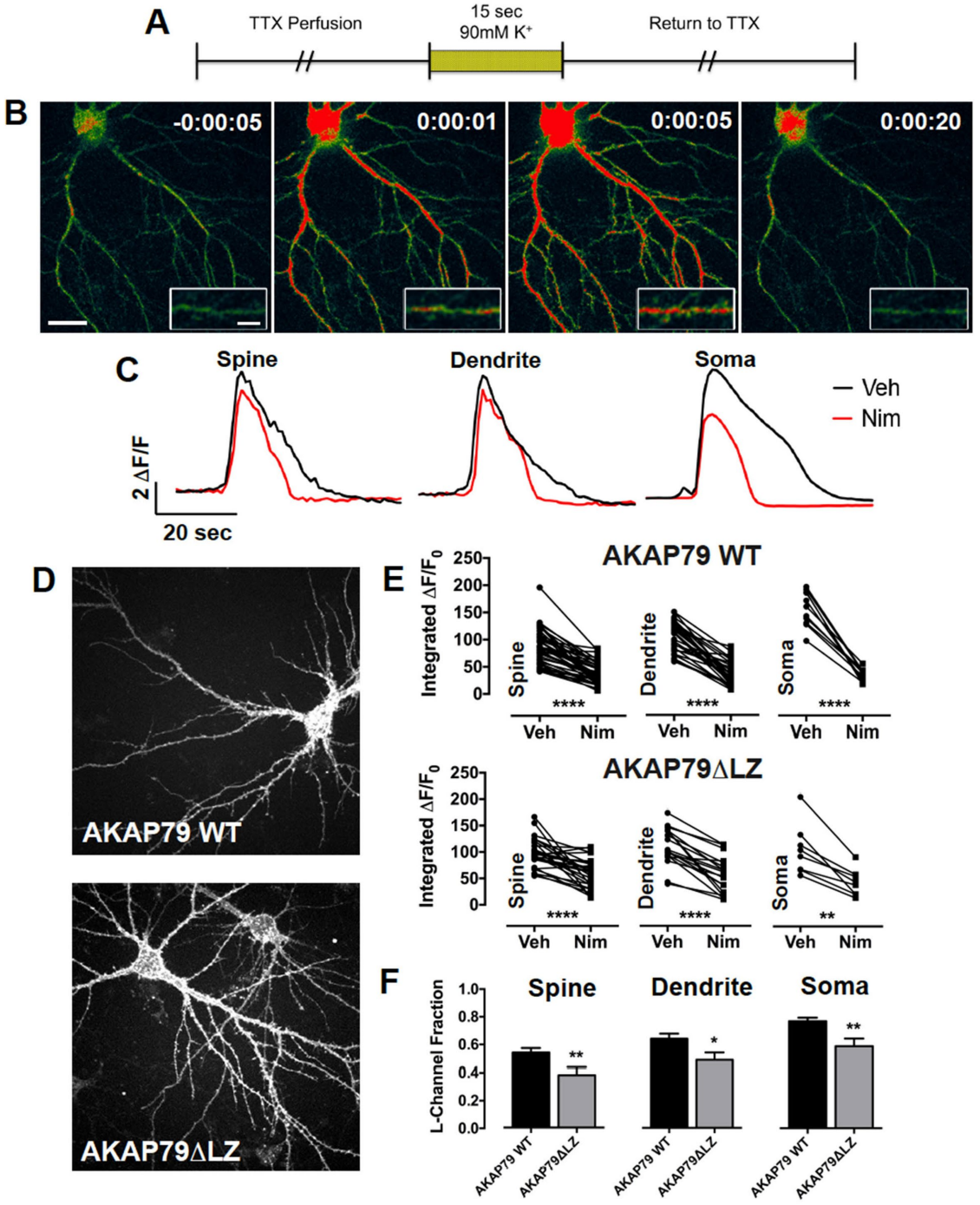

FIGURE 2: Reduced depolarization-triggered Ca^{2+} transients in neurons expressing AKAP79ΔLZ. (A) Schematic of the 90 mM K^+ depolarization protocol used to trigger LTCC Ca^{2+} influx. (B) Time course of GCaMP6f Ca^{2+} indicator fluorescence change, shown in pseudocolor, in response to K^+ depolarization in a cultured rat neuron expressing AKAP150 shRNA and AKAP79WT–mCh. (C) Fluorescence changes measured in the spine, in the dendrite, and at the cell soma of a rat neuron either under control conditions (Veh, black) or in the presence of the LTCC antagonist nimodipine (Nim, red). (D) Representative live-cell images of DIV14–16 rat neurons expressing AKAP150 shRNA, GCaMP6f, and either AKAP79WT–mCh or AKAP79ΔLZ–mCh (white). (E) Quantification of integrated GCaMP6f fluorescence change over time under control conditions or after bath application of Nim. (F) Comparison of the mean LTCC fraction of the total GCaMP6f fluorescence change (****$p < 0.0001$, **$p < 0.01$, *$p < 0.05$; paired *t* test [panel E] or ANOVA with Dunnett's post hoc test [panel F]; $n = 10–39$).

were scaled to the peak inward-current amplitude for visual comparison of inactivation rates. Ca^{2+} currents were fitted to a double exponential function (τ_{fast} = CDI, τ_{slow} = voltage-dependent inactivation) to estimate the rate of CDI (τ_{fast}). To determine the density of the Ca^{2+} current, the peak Ca^{2+} current (pA) was divided by cell capacitance (pF), which is a measure of cell surface area (Figure 3G). In control rat neurons, LTCC CDI and current density were consistent with published values for LTCCs (Figure 3C). As we have previously

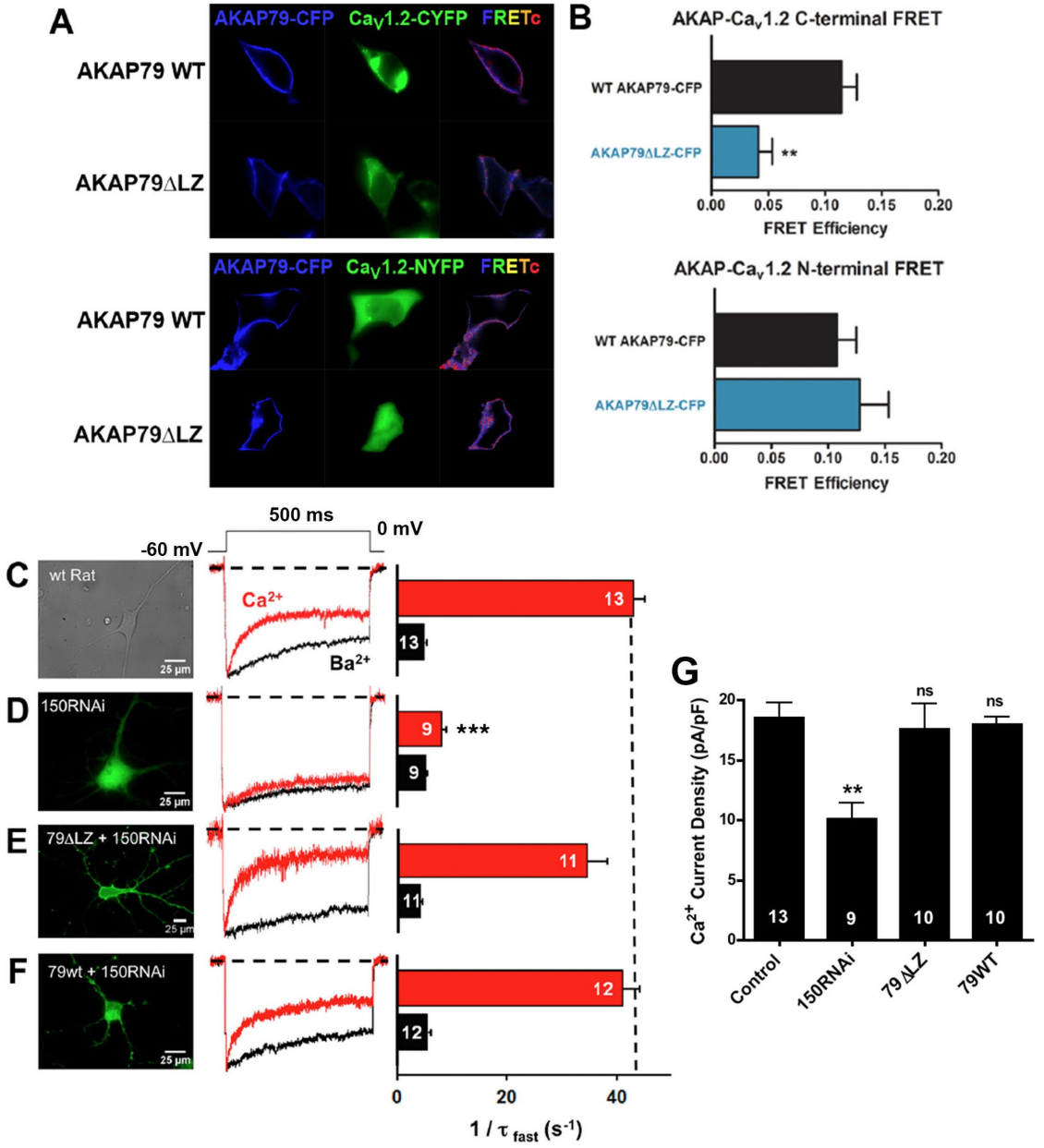

FIGURE 3: The AKAP79/150 LZ motif partially regulates association with the C-terminus of $Ca_V1.2$ but not LTCC current density or Ca^{2+}-dependent inactivation in neurons. (A) tsA-201 cells cotransfected with C- or N-terminally YFP-tagged $Ca_V1.2$ (FRET acceptor, green) and WT or ΔLZ AKAP79–CFP (FRET donor, blue). Corrected FRET (FRETc) shown in pseudocolor gated to CFP. (B) Quantification of apparent FRET efficiency measured between C- or N-terminally YFP tagged $Ca_V1.2$ and WT or ΔLZ AKAP79–CFP (**$p < 0.01$, unpaired t test). (C–F, Left) Images of DIV3-4 cultured rat neurons either untransfected (top; transmitted light) or transfected with AKAP150 shRNA and GFP or rescued with AKAP79WT–GFP (79wt) or AKAP79ΔLZ–GFP (79ΔLZ) (bottom; fluorescence). (Center) Superimposed, normalized records of pharmacologically isolated L-channel Ca^{2+} (red) or Ba^{2+} (black) currents. (Right) Mean inactivation rates (1/τ) in Ca^{2+} (red) or Ba^{2+} (black). (G) Measurements of Ca^{2+} current density from a subset of the neurons in C–F. Number of cells recorded per condition (n) is noted on each bar for panels C–G (***$p < 0.001$,**$p < 0.01$; ANOVA with Dunnett's post hoc test). Data expressed as mean ± SEM. Scale bars = 10 µm.

reported (Oliveria *et al.*, 2012; Dittmer *et al.*, 2014), knockdown of endogenous AKAP150 by shRNA virtually eliminated CDI (Figure 3D) and led to a reduction in LTCC current density (Figure 3G), consistent with our previous observation that decreased LTCC function results from a loss of basal PKA phosphorylation (Dittmer *et al.*, 2014; Murphy *et al.*, 2014). However, reintroduction of either AKAP79WT or AKAP79ΔLZ rescued both CDI and current density, suggesting that the LZ motif of AKAP79 is not required for normal AKAP-mediated regulation of LTCC function or expression in hippocampal neurons (Figure 3, E–G). Thus, despite downstream global LTCC Ca^{2+} signals being somewhat reduced by the AKAP79ΔLZ mutant, local Ca^{2+} signaling in the LTCC nanodomain, which is required for CaN-dependent control of CDI, remains normal. Importantly, our previous work showed that this EGTA-insensitive LTCC nanodomain Ca^{2+} signaling is also most important for CaN–NFAT signaling in hippocampal neurons (Oliveria *et al.*, 2007).

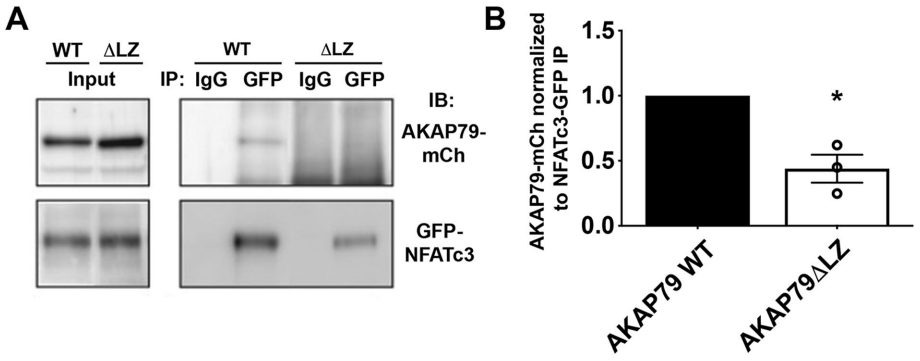

FIGURE 4: AKAP79 and NFATc3 interact in an LZ motif-dependent manner. (A) In tsA-201 cells, anti-GFP–NFATc3 coimmunoprecipitation (IP) of AKAP79–mCh, detected by immunoblotting with anti-RFP/mCh antibody (IB), is reduced in the presence of the AKAP79ΔLZ mutation. IgG = IP with nonimmune immunoglobulin. (B) IP efficiency is quantified by normalization of anti-AKAP79-mCh to anti-GFP-NFATc3 IP band intensity (*$p < 0.05$; unpaired *t* test; $n = 3$).

Co-IP of AKAP79 and NFATc3 is mediated by the AKAP79 LZ motif in tsA-201 cells

While global LTCC-dependent Ca^{2+} signals are moderately altered in AKAP79ΔLZ-expressing neurons, our CDI results do not support a loss of channel function as the reason for the reduction in NFAT signaling in neurons expressing AKAP79ΔLZ. Interestingly, in cardiac myocytes, another member of the AKAP family, mAKAPβ, has been shown to bind to NFATc3, facilitating dephosphorylation of the transcription factor by CaN (Li *et al.*, 2010). This led us to consider whether AKAP79/150 may recruit NFAT to the LTCC signaling complex, where NFAT could respond to local CaN activation. To address this possibility, we coexpressed GFP-NFATc3 and AKAP79-mCh in tsA-201 cells. Pull-down of GFP–NFATc3 using an anti-GFP polyclonal antibody and immunoblotting for AKAP79–mCh with an anti–red fluorescent protein monoclonal antibody demonstrated that AKAP79 and NFATc3 are indeed part of a complex (Figure 4A). It follows that if NFAT recruitment to the LTCC nanodomain is required for efficient NFAT activation by AKAP-anchored CaN, then the impairment in NFAT signaling in AKAP79ΔLZ-expressing neurons may result from loss of this AKAP–NFAT interaction. To test whether the AKAP79 LZ motif regulates the AKAP–NFAT interaction, we coexpressed GFP–NFATc3 and AKAP79ΔLZ–mCh (Figure 4B) and found that AKAP79ΔLZ–NFAT coimmunoprecipitation was strongly reduced (~56%), suggesting that the AKAP79 LZ motif plays a role in mediating an either direct or indirect physical interaction between AKAP79/150 and NFATc3.

AKAP150 regulates NFATc3 mobility in neuronal dendrites and somata

When LTCCs are overexpressed in excitatory neurons, they form clusters that colocalize with AKAP79/150 and exhibit limited lateral diffusion (Di Biase *et al.*, 2008); therefore, disrupting an AKAP-mediated physical association between NFATc3 and the LTCC signaling complex might result in a detectable change in the mobility characteristics of the transcription factor in neurons. To investigate this possibility, we chose two complementary fluorescence-based techniques, fluorescence recovery after photobleaching (FRAP) and fluorescence correlation spectroscopy (FCS; Magde *et al.*, 1972; Axelrod *et al.*, 1976), to measure the impact of AKAP79/150 on the mobility of sGFP2–NFATc3 in neurons. In our FRAP experiments, along with the sGFP2-NFATc3 constructs, we expressed the pSilencer plasmid or AKAP150 shRNA. Another set of measurements were taken from cultures where, in addition to the AKAP150 shRNA, a rescue construct of either AKAP79WT–mCh or AKAP79ΔLZ–mCh was coexpressed. Individual dendritic spines in neurons that had been preincubated with TTX (1 μM) for 15–30 min were targeted for selective photobleaching and imaged every 3 s over 3 min to track fluorescence recovery. Recovery traces were normalized using the method described by Phair and Misteli (2000). Owing to the high noise levels, rather than fitting recovery curves from individual spines, the pooled traces were averaged and fitted with a model describing single-exponential recovery (see *Materials and Methods*). The immobile fraction (on the time scale of our measurements) in spines of sGFP2–NFAT in neurons expressing either pSilencer (Figure 5A) or AKAP150 shRNA plus the AKAP79WT rescue construct (Figure 5B) was markedly higher (~36%) than what was observed in neurons coexpressing just the AKAP150 shRNA construct or shRNA with AKAP79ΔLZ (Figure 5C) (~18% and ~10%, respectively). There was also a moderate increase in the kinetic speed of recovery for AKAP79ΔLZ (decrease in τ_{half} recovery).

Our FRAP experiments were targeted at dendritic spines, as their small compartment size facilitated bleaching an isolated pool of GFP fused to the NFATc3 protein. However, recent work from our lab has demonstrated that the predominant source of NFATc3 translocating to the nucleus following neuronal stimulation is the somatic pool (Wild *et al.*, 2019). Therefore, we sought a means to detect evidence of an association between NFATc3 and the AKAP–LTCC complex, specifically along the somatic plasma membrane. Owing to the large cytoplasmic fraction of sGFP2–NFATc3 in the soma, coupled with our inability to restrict the bleaching/recovery area to the plasma membrane alone, we anticipated that the fast fluorescence recovery of cytoplasmic sGFP2–NFATc3 could overwhelm any changes in NFAT mobility that might result from a disruption of its association with the AKAP. Thus, we reasoned that fluorescence correlation spectroscopy (FCS) might be more capable of detecting an effect. FCS is a technique that yields quantitative information on protein mobility in living cells by measuring intensity fluctuations produced by fluorescent molecules diffusing through a confined detection volume. Qualitatively, we observed a clear leftward shift in the median normalized autocorrelation (AC) curve for sGFP2–NFATc3 with the coexpression of the AKAP150 shRNA/AKAP79ΔLZ–mCh relative to that for sGFP2–NFATc3 expressed with pSilencer/AKAP79WT–mCh (Figure 5D), suggesting that disruption of the AKAP79 LZ motif increases NFAT mobility in the soma. AC curves from individual measurement sets (Supplemental Figure 1) were fitted with a model describing two blinking elements and one component due to three-dimensional diffusion (see *Materials and Methods* for a more detailed description; Figure 5E). There was a clear distinction in both the distribution and the median for the two conditions measured: 0.79 $\mu m^2/s$ (25–75% IQR 0.42 $\mu m^2/s$, 1.22 $\mu m^2/s$) for pSilencer/WT; 1.11 $\mu m^2/s$ (0.69 $\mu m^2/s$, 1.62 $\mu m^2/s$) for 150 shRNA/ΔLZ (see Supplemental Table 1 for a full list of fitted parameters and their values). We also took FCS measurements from secondary dendritic shafts in neurons expressing sGFP2–NFATc3 along with either pSilencer or the AKAP150 shRNA construct, and

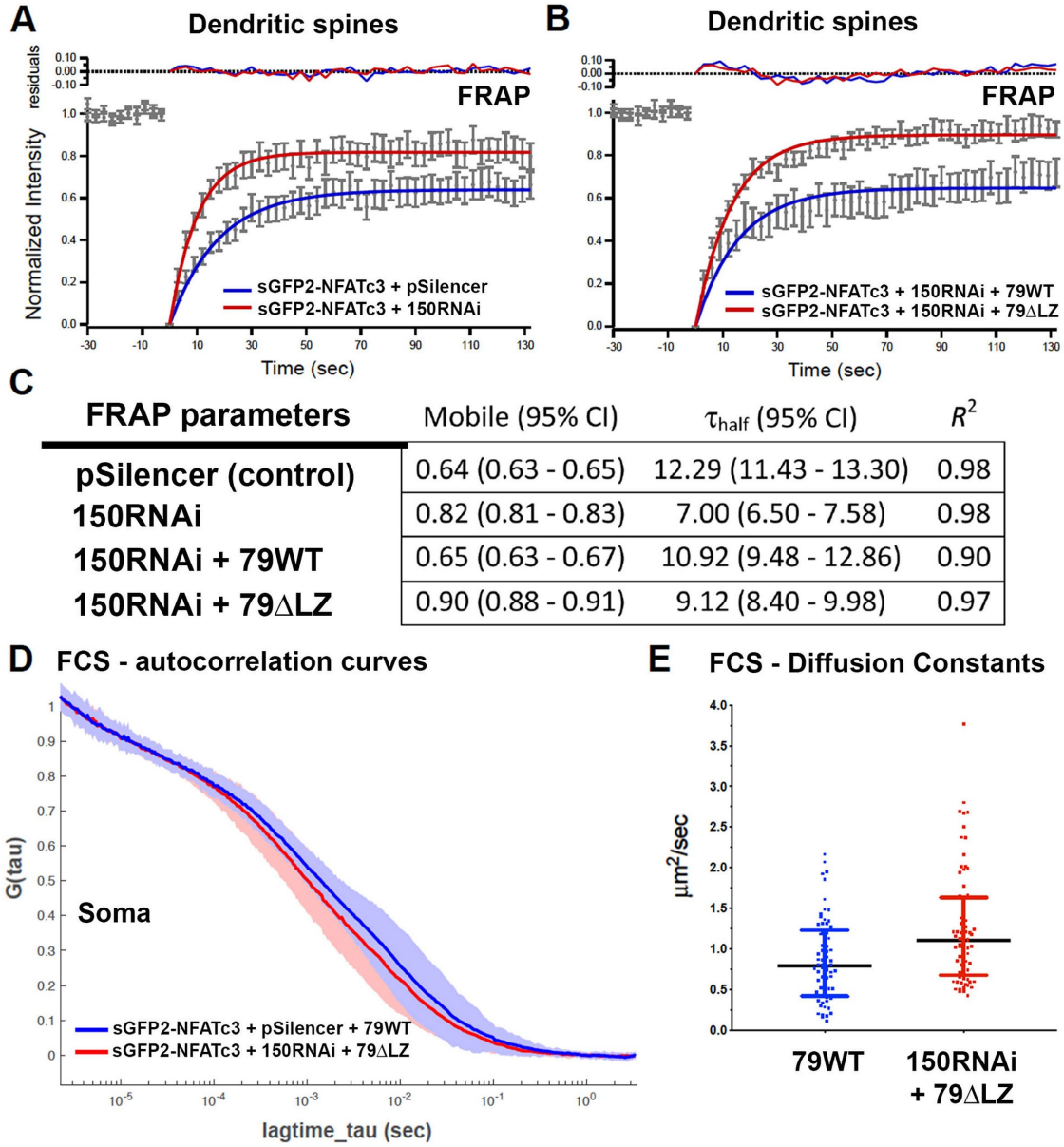

FRAP parameters	Mobile (95% CI)	τ_{half} (95% CI)	R^2
pSilencer (control)	0.64 (0.63 - 0.65)	12.29 (11.43 - 13.30)	0.98
150RNAi	0.82 (0.81 - 0.83)	7.00 (6.50 - 7.58)	0.98
150RNAi + 79WT	0.65 (0.63 - 0.67)	10.92 (9.48 - 12.86)	0.90
150RNAi + 79ΔLZ	0.90 (0.88 - 0.91)	9.12 (8.40 - 9.98)	0.97

FIGURE 5: Deletion of the AKAP79 LZ motif leads to an increase in NFATc3 mobility in neurons. Mean normalized fluorescence recovery curves (± SEM error bars) from FRAP experiments on dendritic spines, fitted with a single exponential (gray markers: experimental data means; color lines: fits and residuals). (A) sGFP2–NFATc3 plus either pSilencer (bottom, blue trace; $n = 32$ spines, 2–3 spines per cell, four separate neuronal preps) or AKAP150shRNA (top, red trace; $n = 27$ spines, 2–3 spines per cell, three separate neuronal preps). (B) sGFP2-NFATc3 and AKAP150shRNA plus either the AKAP79WT–mCh (bottom, blue trace; $n = 21$ spines, 2–3 spines per cell, five separate neuronal preps) or AKAP79ΔLZ–mCh rescue (top, red trace; $n = 34$ spines, 2–3 spines per cell, four separate neuronal preps) constructs. (C) Returned fit parameters (±95% confidence interval) and goodness of fit metric (R^2) for each condition. (D) Median FCS AC curves for sGFP2–NFATc3 plus either pSilencer and AKAP79WT–mCh (blue, rightmost trace; $n = 70$ measurement sets, 2–4 sets per cell, four independent neuronal preps) or AKAP150shRNA and AKAP79ΔLZ–mCh (red, leftmost trace; $n = 69$ measurement sets, 2–4 sets per cell, four independent neuronal preps). Shaded areas show 25–75% IQR. (E) Fitted apparent diffusion coefficients from fits for individual FCS AC measurements of sGFP–NFATc3 (see *Materials and Methods*), plotted as individual data points. Bars show median values, 0.79 μm²/s for pSilencer+AKAP79WT, 1.11 μm²/s for AKAP150shRNA+AKAP79ΔLZ and 25–75% IQR.

here, also, we observed an overall increase in mobility upon knockdown of AKAP150 (Supplemental Figure 2). Taken together, these FRAP and FCS mobility data support a model where AKAP150, via its LZ domain, functions to restrict the mobility of NFAT, possibly stabilizing it in proximity to LTCC signaling domains in multiple regions of excitatory neurons.

DISCUSSION

Dynamic AKAP79/150 regulation of LTCC phosphorylation and function has a well-established role in excitation–transcription coupling through activation of NFAT signaling (Woolfrey and Dell'Acqua, 2015; Wild and Dell'Acqua, 2018). Our previous work demonstrated that NFAT signaling requires both basal LTCC phosphopriming by

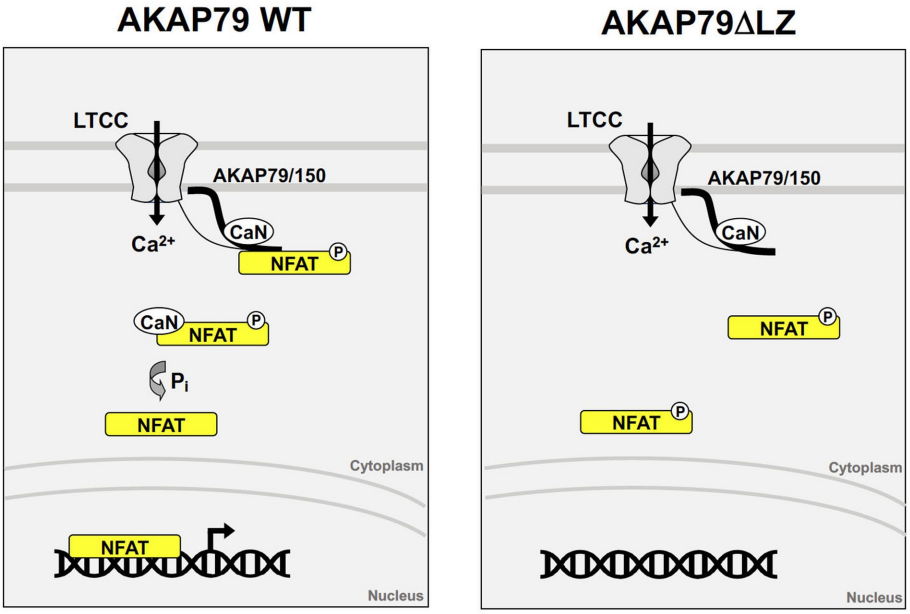

FIGURE 6: Local Ca^{2+} influx through LTCCs leads to dephosphorylation and actuation of NFAT by the Ca^{2+}-dependent phosphatase CaN. Proposed model of NFAT signaling to the nucleus requiring recruitment of both CaN and NFAT to the LTCC by AKAP79 (left). In the absence of the AKAP79 LZ motif, measures of NFAT–AKAP interaction are reduced, including co-IP, FRAP, and FCS. Additionally, NFAT is unable to translocate to the nucleus and regulate transcription (right).

AKAP-anchored PKA and AKAP-mediated localization of CaN for efficient Ca^{2+}–CaM activation near the channel pore (Li *et al.*, 2012; Oliveria *et al.*, 2012; Dittmer *et al.*, 2014; Murphy *et al.*, 2014). Our goal in this study was to gain new insight into how LTCCs and NFAT signaling are regulated by the AKAP79/150 C-terminal LZ domain, which is thought to serve as the primary anchoring site on AKAP79 for the LTCC. However, we did not detect significant perturbation of the AKAP79–LTCC complex due to deletion of the AKAP79 LZ motif, an observation that is in agreement with previous studies indicating that there are other secondary interactions that help stabilize this complex (Hall *et al.*, 2007; Oliveria *et al.*, 2007; Di Biase *et al.*, 2008). Nonetheless, our studies revealed that the C-terminal LZ motif of AKAP79/150 is involved in functional coupling of LTCC activity to CaN–NFAT signaling, likely through transient recruitment of NFAT to the AKAP–LTCC complex, thus adding new mechanistic insight into how very local elevations of the ubiquitous second messenger Ca^{2+} can efficiently activate the NFAT signaling pathway (Figure 6).

It has been known for more than two decades that LTCCs have an advantage over other voltage-gated Ca^{2+} channels in coupling neuronal membrane depolarization to transcription (Murphy *et al.*, 1991; Bading *et al.*, 1993; Graef *et al.*, 1999). In our past experiments, we found that engagement of NFAT signaling in response to Ca^{2+} entry relies on AKAP scaffold recruitment of CaN near the mouth of the intracellular pore of the LTCC (Oliveria *et al.*, 2007; Li *et al.*, 2012; Murphy *et al.*, 2014). In the current study, we provide new evidence, in the form of fluorescence-based mobility data from two complementary techniques, FRAP and FCS, that NFATc3 is also part of this local signaling complex and is likely recruited via the LZ motif on AKAP79/150. Additional, biochemical co-IP of AKAP and NFAT, which is disrupted by deletion of the AKAP LZ domain, further supports a possible direct or indirect physical interaction between these two proteins.

Deletion of the AKAP LZ motif did not completely disrupt the AKAP–LTCC complex, as shown by FRET microscopy. However, deletion of the LZ domain moderately decreased depolarization-evoked LTCC bulk cytosolic Ca^{2+} signals measured in the spines, dendrites, and cell bodies of hippocampal neurons. Yet, in contrast, LZ deletion did not affect AKAP79 regulation of channel kinetics, current density, or CDI in whole-cell voltage clamp recordings, suggesting that local LTCC Ca^{2+}–CaN signaling is normal. Thus, while we cannot completely rule out a contribution by decreased LTCC bulk cytosolic Ca^{2+} signals to the NFAT signaling defect observed for the ΔLZ mutant, these modest reductions (~15%) in bulk cytosolic Ca^{2+} alone cannot account for the very strong reduction of LTCC–NFAT signaling in neurons expressing AKAP79ΔLZ. In particular, our previous work demonstrated that the fast Ca^{2+} chelator BAPTA, which can buffer both bulk, cytoplasmic Ca^{2+} and LTCC nanodomain Ca^{2+}, disrupted LTCC–CaN coupling to NFAT, while the slow Ca^{2+} chelator EGTA, which can only buffer bulk, cytoplasmic Ca^{2+}, had no effect (Oliveria *et al.*, 2007). Therefore, local Ca^{2+} influx at the mouth of the channel is primarily responsible for initiating NFAT signaling to the nucleus, and our electrophysiology experiments suggest that local Ca^{2+} signaling and AKAP79 regulation of the LTCC phosphorylation state are intact in neurons expressing AKAP79ΔLZ. Thus, our data indicate an additional role for the LZ domain in regulation of NFAT signaling through mediating AKAP79–NFAT binding.

In this model (Figure 6), the key role of the AKAP LZ motif in regulating NFATc3-mediated excitation–transcription signaling is likely to transiently recruit the transcription factor to the LTCC signaling complex, near the mouth of the intracellular pore. This AKAP co-recruitment of NFAT with its upstream activators, the LTCC and CaN, could facilitate signaling that would otherwise be inefficient without such local sequestration of second messenger activator, enzyme, and substrate. The structural nature of the AKAP–NFAT complex, and whether it is, as we speculate, a direct interaction, warrant further study. In immune and other cells, efficient transcriptional activation of a number of NFAT genomic targets requires cooperative DNA binding with the transcription factor AP-1. AP-1 is a heterodimer of fos and jun, which bind to each other through a canonical LZ coiled-coil interaction (Kouzarides and Ziff, 1988; Landschulz *et al.*, 1988; Sassone-Corsi *et al.*, 1988). A quaternary crystal structure including NFAT and AP-1 bound to DNA has been described in which a hydrophobic beta-sheet of the rel homology region of NFAT binds to the fos/jun LZ coiled-coil structure (Chen *et al.*, 1998). It is tempting to speculate that NFAT and AKAP79 may directly interact as part of the LTCC signaling complex via the AKAP–LTCC modified LZ coiled-coil in a manner similar to that described for the fos–jun–NFAT interaction in the nucleus. It is also possible that AKAP79, shown to dimerize in vitro (Gao *et al.*, 2011; Gold *et al.*, 2011), may form a coiled-coil C-terminal structure to provide NFAT docking even in the absence of the LTCC. While such detailed structural insight into the AKAP–NFAT interaction is lacking at this time, our model proposed here for AKAP-mediated

recruitment of NFAT to the LTCC nanodomain provides an attractive explanation for the privileged role of LTCCs over other neuronal Ca^{2+} sources in NFAT signaling.

MATERIALS AND METHODS

Animal care and use

All animal procedures were conducted in accordance with National Institutes of Health (NIH)-United States Public Health Service guidelines and with the approval of the University of Colorado Denver Institutional Animal Care and Use Committee.

Immunoprecipitation and immunoblotting

For GFP–NFATc3 immunoprecipitation (IP), tsA-201 cells were homogenized in lysis buffer (50 mM Tris, pH 7.5, 150 mM NaCl, 5 mM EDTA, 5 mM EGTA, 5 mM NaF, 2 mg/ml leupeptin, 2 mg/ml pepstatin, 1 mM benzamidine, and 1 mM 4-(2-aminoethyl)benzenesulfonyl fluoride hydrochloride [AEBSF]) and incubated on ice for 20 min in the presence of 1% Triton X-100. Lysates were spun for 20 min at 20,800 × *g*. A portion of 10% of supernatant was reserved for gel loading of whole cell extract. The remaining supernatant was split evenly into two to three samples, receiving either 5 µg rabbit anti-GFP or 5 µg nonimmune rabbit anti–immunoglobulin G (IgG) antibodies (control). Samples were incubated overnight at 4°C with end-over-end rotation, followed by 1 h in protein A Sepharose beads, before extensive washing. The entire IP or 10 µg whole extract (WE/input) was resolved on Tris-SDS gels and transferred in 20% methanol to PVDF membranes. Primary rabbit anti-RFP/mCh (1:2000) or rabbit anti-GFP (1:5000) antibody was incubated with the membranes for a minimum of 2 h. Immunoblotting detection was then performed with horseradish peroxidase (HRP)-coupled secondary antibodies (Bio-Rad; 1:1000) followed by enhanced chemiluminescence (ECL; WestPico or West Dura Chemiluminescent Substrate; Pierce). Chemiluminescence was imaged using an Alpha Innotech Fluorchem gel documentation system.

Live-cell FRET microscopy in tsA-201 cells

Cultured tsA-201 cells were plated on glass coverslips in DMEM + 10% fetal bovine serum and 1% penicillin/streptomycin, grown for 48 h, and then transfected using Turbofect (Thermo Scientific) with cDNA plasmids encoding AKAP79 WT or ΔLZ-CFP and YFP–$Ca_V1.2$ or $Ca_V1.2$–YFP (rabbit Cav1.2) as previously described (Oliveria *et al.*, 2007). Living cells were imaged at room temperature 24–48 h posttransfection using an Axiovert 200M microscope with a 63× plan-apo/1.4 NA objective, Lambda XL illumination (Sutter Instruments), Coolsnap-HQ CCD camera (Roper Scientific), and Slidebook 4.2–5.5 software. Three-filter FRET images were captured with 2 × 2 binning and processed, and sensitized FRET efficiency was measured as described previously (Oliveria *et al.*, 2003, 2007), with more details provided below.

Quantification of live-cell FRET microscopy in tsA-201 cells

CFP, YFP, and CFP-YFP FRET fluorescence were captured in single *xy* planes in living cells using the following excitation and detection scheme: 1) CFPexcitation/CFPemission, 2) YFP excitation/YFPemission, and 3) CFPexcitation/YFPemission (rawFRET). After background subtraction, FRET corrections were applied across entire images for CFP bleed-through (54% for AKAP79-CFP) and YFP cross-excitation (2% for YFP-$Ca_V1.2$) to yield an image of corrected FRET (FRETc), using the equation FRETc = rawFRET − (0.54 × AKAP79-CFP) − (0.02 × YFP-$Ca_V1.2$). Spectral bleed-through corrections were determined by expressing either AKAP79–CFP or YFP–$Ca_V1.2$ constructs alone in tsA-201 cells and averaging CFP, YFP, and rawFRET intensities across many cells. AKAP79–CFP bleed-through detected as YFP emission and YFP–Cav1.2 cross-excitation by the CFP excitation filter measured in the FRET channel were calculated as FRET emission/AKAP79–CFP emission and FRET emission/YFP–$Ca_V1.2$ emission, respectively. FRETc was then gated to the CFP donor channel to create a FRETc/CFP pseudocolor image of relative FRET intensity in the cell. Mean CFP, YFP, and raw FRET fluorescence intensities were measured by mask analysis of membrane regions (or the cytoplasm for linked CFP–YFP) in Slidebook 4.0–5.5 as described previously (Oliveria *et al.*, 2003, 2007; Li *et al.*, 2012). Apparent FRET efficiency (FRETeff) values were calculated from these mean intensities using the equation FRETeff = FRETc/((0.02 × YFP) × 10.6) for a 1:1 complex, where FRETc is the emission from YFP due to FRET, 0.02 × YFP is the emission from YFP directly excited with the FRET filter cube, 10.6 is a factor relating CFP excited to YFP excited with the FRET filter cube, and (0.02 × YFP) × 10.6 is therefore the maximum sensitized YFP emission possible if every excited CFP transfers its excitation to the associated YFP (Erickson *et al.*, 2001, 2003; Oliveria *et al.*, 2007; Li *et al.*, 2012)

Primary culture of rat hippocampal neurons

Rat hippocampal neurons were prepared as described previously (Gomez *et al.*, 2002). Briefly, hippocampi were dissected from postnatal day 0–2 Sprague Dawley rats. Neurons were plated at medium density (125,000 cells/ml) on poly-D-lysine–coated glass coverslips. Neurons were cultured in Neurobasal-A (NB) medium supplemented with 2% B-27, 1% Glutamax, and 1% penicillin/streptomycin, with mitotic inhibitors added at DIV 4 or 5; thereafter, neurons were fed every 4 or 5 d. All cell culture media and supplements were obtained from ThermoFisher Scientific.

Transfection of rat primary hippocampal neurons

DIV 11–13 neurons were transfected using Lipofectamine 2000 (Life Technologies). Each transfection reaction contained 4–8 µg total plasmid encoding cDNA/shRNA. For each 18- or 25-mm coverslip in 12- or 6-well plates, 4 or 8 µl of Lipofectamine was added, respectively. Briefly, NB and Lipofectamine or NB and plasmid DNA were combined and incubated for 5 min in separate tubes at room temperature. After 5 min, the Lipofectamine and DNA tubes were combined at room temperature and incubated for 20 min to create Lipofectamine/DNA complexes. During the 20-min incubation, half of the medium was removed from the cultured cells and mixed with fresh NB (+2% B27, 1% Glutamax, and 1% penicillin/streptomycin) and saved. Following the 20-min incubation, the Lipofectamine/DNA mixture was added dropwise to the cultures and allowed to incubate for 1.5–2.0 h at 37°C, 5% CO_2. After incubation, Lipofectamine-containing media was replaced with conditioned NB culture media. Neurons were then returned to the incubator at 37°C, 5% CO_2 and imaged at DIV 12–14. Owing to the low concentration requirements, for the FCS experiments, a titration range of 200 ng per well and 500 ng per well (25 mm coverslips) of sGFP2-NFATc3 DNA (Wild *et al.*, 2019) was utilized for the transfections.

GFP–NFATc3 translocation in hippocampal neurons

As previously described (Murphy *et al.*, 2014), DIV 12–14 cultured hippocampal neurons expressing GFP–NFATc3 (24–48 h posttransfection) were placed in a Tyrode's salt solution (in mM: 135 NaCl, 5 KCl, 2 $CaCl_2$, 1 $MgCl_2$, 25 HEPES, 10 glucose, and 0.1% BSA, pH 7.4) plus 1 µM TTX (Tocris) at 37°C for 0.5–1.0 h to dampen spontaneous activity and reduce basal levels of nuclear GFP–NFATc3. Subsequent to TTX preincubation, cells were depolarized for 3 min

in isotonic 50 mM KCl Tyrode's solution to activate LTCCs. Next, the cells were allowed to recover for 10 min in control Tyrode's solution containing 1 μM TTX at 37°C, 5% CO_2. Cells were then washed in PBS, fixed (3.7% formaldehyde in PBS), permeabilized (0.1% Triton X-100 in PBS), and immunostained to detect transfected GFP–NFATc3. Primary antibodies (mouse anti-GFP and rabbit anti-RFP/mCh; Abcam) were diluted 1:500 in 3% BSA in PBS, applied directly to coverslips, and incubated for 2 h at room temperature. Cells were washed three times in PBS, and secondary antibodies (goat anti-mouse Alexa Fluor 488 and goat anti-rabbit Alexa Fluor 568; Life Technologies) were diluted 1:500 in 3% BSA in PBS, applied directly to coverslips, and incubated for 1 h at room temperature. Coverslips were then washed three times in PBS before being mounted on glass slides with Pro-long Gold Antifade mountant containing 4′,6-diamidino-2-phenylindole (DAPI; ThermoFisher).

Measurement of NFAT transcriptional reporter expression

NFAT transcriptional reporter assays were carried out essentially as described previously (Li *et al.*, 2012). Rat neurons (12 DIV) were transfected with the 3xNFAT/AP1-CFPnls fluorescent reporter plasmid, pSilencer or AKAP150 shRNA, and either YFP, AKAP79-YFP WT, or ΔLZ plasmids, as described above. At 4 h after transfection, 1 μM TTX was added in conditioned culture medium for 16 h at 37°C, 5% CO_2, to dampen spontaneous activity and decrease basal CFP reporter expression. After this TTX pretreatment, neurons were subjected to a 5-min wash in control Tyrode's, followed by 3 min depolarization with isotonic 90 mM KCl containing Tyrode's or control Tyrode's, and then an additional 5-min wash in control Tyrode's before being returned to conditioned media containing 1 μM TTX for 16 h at 37°C, 5% CO_2. Neurons expressing the 3xNFAT/AP1–CFPnls reporter were then fixed in 3.7% formaldehyde in PBS, permeabilized with 0.1% Triton X-100 in PBS, stained with a 1 μM solution of propidium iodide (PI) to visualize the nucleus, and mounted onto glass slides as above with Pro-long Gold Antifade (but without DAPI).

Fluorescence microscopy and quantitative image analysis of fixed cells

Fluorescence images were captured using an Axiovert 200M microscope (Carl Zeiss) with a 63× plan-apo/1.4 numerical aperture (NA) objective, 300 W xenon illumination (Sutter Instruments), a Coolsnap-HQ2 charge-coupled device (CCD) camera (Roper Scientific), and Slidebook 4.2–5.5 software (Intelligent Imaging Innovations). AKAP79-mCh or YFP, GFP-NFATc3, CFP, DAPI, and/or PI fluorescence was imaged by acquiring 5-μm *z* stacks of *xy* planes at 0.5-μm intervals. Planes were deblurred using nearest-neighbor deconvolution and sum or maximum intensity projected into two-dimensional images. GFP-NFATc3 nucleus-to-cytoplasm fluorescence intensity ratios and CFPnls transcriptional reporter activity were quantified as described previously (Murphy *et al.*, 2014) using mask analysis in Slidebook 4.2–5.5 (Smith *et al.*, 2006; Li *et al.*, 2012). Statistical comparisons of nucleus/cytoplasm ratios and mean CFP fluorescence in the nucleus across groups were carried out using GraphPad Prism 4.0–5.0 (analysis of variance [ANOVA] or Student's *t* test as indicated in the figure legends).

Calcium imaging and analysis in hippocampal neurons

Fast confocal imaging was performed using an EC Plan-Neofluar 40×/1.30 NA oil objective on an Axio-Observer Z1 microscope (Carl Zeiss) coupled to a CSU-X1 spinning disk (Yokogawa), an Evolve 16-bit electron-multiplying CCD camera (Photometrics), and Slidebook 5.0–5.5 software. DIV 12–15 neurons were grown on glass coverslips and transfected 24–48 h before imaging. Neurons were transfected with pSilencer (empty vector control) or AKAP150 shRNA plus mCh, AKAP79WT–mCh, or AKAP79ΔLZ–mCh, and GCaMP6f (Addgene 40755) as indicated using Lipofectamine 2000 (Invitrogen). Coverslips were mounted in an imaging chamber (Warner Instruments RC-21BDW) and perfused in normal Tyrode's saline containing TTX and vehicle or nimodipine for the duration of the experiment. Neurons were maintained at 34°C, whereas sequential single *xy* planes were acquired at 0.5 Hz for 1 or 2 min, encompassing a 15- or 30-s 90-mM K^+ perfusion. Changes in GCaMP6f fluorescence were measured for regions of interest in spines, primary dendrites, or in the soma using Slidebook 5.0–5.5

Short-term cultured hippocampal neurons for patch-clamp recording

Primary hippocampal neurons were prepared from neonatal Sprague Dawley rats (P0–3), as described above and previously (Gomez *et al.*, 2002; Smith *et al.*, 2006). For AMAXA Nucleofector transfection, P0–2 neurons were resuspended at (3–4) × 10^6 cells/transfection, electroporated with 6–8 μg of total plasmid DNA (AKAP79 WT-GFP, ΔLZ-GFP, GFP alone, and 150RNAi), plated at (0.25–0.5) × 10^6 cells/25 mm glass coverslip, and maintained for 3–5 DIV.

Whole-cell patch-clamp recording

Heat-polished borosilicate patch pipettes (4–8 MΩ, in the bath) and an Axopatch 1D amplifier (Molecular Devices) were used to voltage-clamp currents. Series resistance compensation, capacitance cancellation, and leak subtraction were employed. Records were filtered at 2 kHz and sampled at 10 kHz using Pulse software (HEKA). The whole-cell pipette contained (in mM) 120 $CsMeSO_4$, 30 TEA-Cl, 10 EGTA, 5 $MgCl_2$, 5 Na2ATP, and 10 HEPES, pH 7.2, with TEA-OH. The bath solution contained 1 μM TTX and (in mM) 125 NaCl, 10 $CaCl_2$ or $BaCl_2$, 5.85 KCl, 22.5 TEA-Cl, 1.2 $MgCl_2$, 10 HEPES (Na), and 11 D-glucose, pH 7.4, with TEA-OH. Transfected neurons were identified by fluorescence from GFP or AKAP79-GFP constructs. Only recordings with an access resistance <10 MΩ were pursued. Currents were evoked by 500-ms step depolarization, once every 15 s, from -60 to 0 mV in Ca^{2+} or Ba^{2+} solutions. Currents were recorded first in Ba^{2+} and then, in the same cell, in Ca^{2+}. In all experiments, continuous fast perfusion (~1 ml/min) with a three-barrel system (SF-77B, Warner Instruments) allowed rapid and complete solution exchanges. L-type currents were isolated from other Ca^{2+} current types by pretreating neurons for 30 min with the long-duration blockers of N- and P/Q-type channels, ω-CTx-GVIA (1 μM) and ω-CTx-MVIIC (5 μM), and by holding neurons at −60 mV during recordings to inactivate T-type and R-type Ca^{2+} channels (Sochivko *et al.*, 2003; Oliveria *et al.*, 2007; Tavalin, 2008). To compare inactivation rates, Ca^{2+} and Ba^{2+} current records obtained from the same neuron were normalized by peak inward amplitude. Inactivation time course was best-fit with a double exponential function (PulseFit software; HEKA). The faster component represents CDI, and the slower corresponds to voltage-dependent inaction. Statistical analyses (ANOVA, Bonferroni posttest) were carried out with SigmaPlot 11 (Systat).

Fluorescence-based mobility measurements in live hippocampal neurons

Primary disassociated hippocampal neuron cultures were transfected at DIV 15 (Lipofectamine transfection system, according to modified manufacture's guidelines) with a plasmid encoding an NFATc3 N-terminal fusion (Wild *et al.*, 2019) of the optimized green fluorescence protein sGFP2 (Kremers *et al.*, 2007) and either a

plasmid encoding RNAi for AKAP150 or the empty pSilencer backbone. In FRAP experiments, additional cultures were transfected with the AKAP150 shRNA construct and either an AKAP79WT-mCh or AKAP79ΔLZ-mCh rescue construct. Imaging was performed two days after transfection (DIV 17). TTX was added to the culture media, to a final concentration of 1 μM, ~30 min before imaging in Tyrode's buffer with 1 mM Mg^{2+}, 1 mM Ca^{2+}, and 1 μm TTX at room temperature.

FRAP acquisition. Confocal FRAP imaging was performed on a 3I Marianas system built around a Zeiss Axiovert 200M inverted microscope equipped with a 63×/1.4 NA oil objective and a Yokagawa CSU-X1 spinning-disk unit. Samples were illuminated with 488-nm excitation light from a 50-mW laser diode, which was directed through a multipass 405/488/561/640 dichroic mirror. Emission light was passed through a bandpass filter before being projected onto the chip of a Photometrics Evolve 512 EMCCD. Camera amplification was set to 1000 and gain set to 3. Image dimensions were 256 × 256 pixels at 0.212 μm per pixel. In total, 55 images were collected at 0.3 Hz (3 s intervals). Excitation power was kept low (5–10%) with a frame integration time of 75–150 ms to minimize the effects of acquisition photobleaching on the fluorescence recovery trace. After the acquisition of the tenth frame (30 s), two successive bleaching pulses with a duration of 2 ms each were delivered to a region of interest (ROI) with pixel dimensions of 5 × 5 via a 3I Vector High Speed Point Scanner.

FRAP processing and analysis. In addition to a raw intensity trace from the FRAP region, $I_{raw}(t)$, a background intensity trace, $I_{bkg}(t)$, was obtained from a ROI outside the cell and a reference trace, $I_{ref}(t)$. The FRAP data were then double-normalized using the method described by Phair and Misteli (2000),

$$I_{nrm} = \frac{\mathrm{ref}_{pre} \cdot \left(I_{raw}(t) - I_{bkg}(t)\right)}{\left(I_{ref}(t) - I_{bkg}\right) \cdot \mathrm{frp}_{pre}}$$

where ref_{pre} and frp_{pre} are the background corrected means of the prebleach time points from the reference and FRAP region intensity traces, respectively. FRAP curves from individual ROIs were vetted for adequate bleaching (≥50% postbleach intensity compared with prebleach intensity) and stability of intensity trace (e.g., traces with distortions due to cellular movement or stage drift were discarded). After screening, normalized curves were then scaled 0–1 and averaged. Standard deviation and standard error of the mean were calculated. Averaged curves were fitted with a single exponential, $\mathrm{FRAP}(t) = A\,(1 - e^{-\tau t})$, where A = mobile fraction and the halftime of full recovery ($t_{1/2}$) = ln 2/τ.

FCS acquisition. FCS was performed on a Zeiss 780 confocal equipped with a ConfoCor 3 module C using an Apochromat 40×/1.2 NA W Korr FCS M27 objective. The objective's correction collar position was optimized by taking measurements from a sample of 20 nM fluorescein (Sigma) and adjusting until maximum count level was reached (~53 kHz). The AOTF transmission for the 488 line of an argon laser was set at 2.0%. The confocal pinhole was set at 1 AU (34 μm), with its position optimized with the same 20-nM fluorescein sample using the automatic adjustment feature in Zeiss's Zen software. Pupil filling was set at 100%. Excitation light was passed through an MBS 488 dichroic; fluorescence emission passed through a diffraction grating with the spectral detection window set to 490–606 nm before reaching a GaAsP array PMT. Binning was set at 0.2 μs; the maximum correlation time was set to 1000 s with 16 tau channels.

The FCS detection volume was estimated by taking a calibration measurement of 20 nM fluorescein, which has a known diffusion coefficient of 425 $\mu m^2 s^{-1}$ (Culbertson *et al.*, 2002). AC curves from these acquisitions were fitted with the standard equation for three-dimensional diffusion, along with a triplet-state blinking component:

$$G(\tau) = \frac{1}{\langle N \rangle} \cdot \left(1 + \left(\frac{T}{1-T}\right) \cdot \exp\left(-\tau/\tau_{trip}\right)\right) \cdot \frac{1}{1 + 4D\tau/\omega_{xy}^2} \cdot \frac{1}{\sqrt{1 + 4D\tau/\omega_z^2}}$$

where D, the diffusion coefficient, was fixed to yield ω_{xy}^2 and ω_z^2, the lateral and axial radii of the detection volume, which were ~0.18 and 1.42 μm, respectively, with some variation between experimental days.

Because FCS relies upon a very low concentration of fluorophore (in the nanomolar range), competition from endogenous (nonfluorescent) proteins is a concern in association experiments, we combined the moderate-to-low coexpression of AKAP79WT–mCh with pSilencer expression versus coexpression of AKAP79ΔLZ–mCh with the AKAP150 shRNA knockdown to either increase the number of potential GFP–NFATc3 binding sites or enhance the competition with residual WT protein. Although this strategy precluded preforming complementary knockdown/rescue experiments, as was done for the FRAP studies in dendritic spines, we were able to use the AKAP79–mCh constructs to mark the plasma membrane of the soma so that we could position the confocally defined detection volume straddling the plane upper membrane (farthest from the coverslip).

Thirteen to 15 sequential 10-s measurements were acquired; a maximum of four sets per cell (each in a different region of the soma) were made.

Secondary dendrites (~1 μm diameter) were selected for FCS measurements with the measurement point placed within a straight section of shaft, away from any prominent branch points. As was the case with the somatic measurements, 15 sequential 10-s acquisitions were acquired from this point; however, for this data set, only one measurement was made per cell.

FCS analysis. The open source software PyCorrFit v.0.83 (Müller *et al.*, 2014) was utilized for initial analysis and fitting. The 15 individual traces and AC curves from each acquisition set were first inspected, and any that showed obvious distortions due to cell movement or pronounced photobleaching were discarded from further analysis. The remaining AC curves (~10–15) were then averaged and the resulting mean AC curve was fitted. In the case of measurements from secondary dendrites, we utilized a model that accounted for the confined geometry of the dendrite, describing one diffusion component and two blinking components: the standard triplet-state blinking in addition to an additional blinking state, likely due to transient protonation of the GFP chromophore, which we have found to be a prominent component of the AC curve in neurons:

$$G(\tau) = A_0 + \frac{1}{n} \cdot \left(1 + \left(\frac{T}{1-T}\right) \cdot \exp\left(-\tau/\tau_{trip}\right)\right) \cdot \left(1 + K_{equ} \exp\left[-\tau/\tau_{qnch}\right]\right) \cdot \frac{1}{\left(1 + \left(\tau/\tau_{diff}\right)^a\right)}$$

The elements of this model are as follows: the returned parameters of note are T and τ_{trip}. describing the molecular fraction blinking due to triplet state transitions and the blinking frequency, K and

τ_{qnch}, describing the kinetics of protonation/deprotonation of the GFP chromophore and the blinking frequency that results from this process, and τ_{diff} and α, describing the average time it takes the fluorescent molecule to traverse the detection volume and an anomalous exponential to account for confined/disrupted diffusion.

For data from neuronal somata, we opted to fit the AC curves with a model that included both blinking states, but where the diffusion component was instead represented by an equation describing three-dimensional diffusion, where κ describes the structural parameter of the detection volume, ω_z^2/ω_{xy}^2,

$$G(\tau) = A_0 + \frac{1}{n}\cdot\left(1+\left(\frac{T}{1-T}\right)\cdot\exp\left(-\tau/\tau_{trip}\right)\right)\cdot\left(1+K_{equ}\exp\left[-\tau/\tau_{qnch}\right]\right)$$
$$\cdots\frac{1}{(1+\tau)/\tau_{diff}}\cdot\frac{1}{\sqrt{1+\tau/k^2\,\tau_{diff}}}$$

This single diffusion component creates a metric (an apparent diffusion coefficient) that is likely a function of a number of elements, perhaps including, but not necessarily restricted to, three-dimensional diffusion of the largely cytoplasmic sGFP2–NFATc3, transient binding/unbinding of sGFP2–NFATc3 to the stabilized AKAP79/150–LTCC complex, and transient binding/unbinding and codiffusion of sGFP2–NFATc3 to/with AKAP79/150 along the plasma membrane. Given this complexity and the relatively low amplitudes of the AC curves (resulting from the difficulty in tuning the transient transfections so that they yield the low, but still detectable, expression levels that are needed for high-quality FCS measurements (see Supplemental Figure 1 and associated legend), it was more feasible to utilize this simpler model, rather than try to describe all the potential behaviors with a more convoluted set of equations.

ACKNOWLEDGMENTS

This research was supported by a grant from the National Institutes of Health (NIH) to M.L.D. (R01 MH102338). FCS imaging experiments were performed in the University of Colorado Anschutz Medical Campus Advanced Light Microscopy Core supported in part by Rocky Mountain Neurological Disorders Core Grant P30 NS048154 and by NIH/National Center for Advancing Translational Sciences Colorado Clinical and Translational Sciences Institute Grant UL1 TR001082. Contents are the authors' sole responsibility and do not necessarily represent official NIH views. Special thanks to Seth F. Oliveria for initial construction and characterization of the AKAP79ΔLZ mutant.

REFERENCES

Axelrod D, Koppel D, Schlessinger J, Elson E, Webb W (1976). Mobility measurement by analysis of fluorescence photobleaching recovery kinetics. Biophys J 16, 1055–1069.

Bading H, Ginty DD, Greenberg ME (1993). Regulation of gene expression in hippocampal neurons by distinct calcium signaling pathways. Science 260, 181–186.

Bauman AL, Soughayer J, Nguyen BT, Willoughby D, Carnegie GK, Wong W, Hoshi N, Langeberg LK, Cooper DM, Dessauer CW, Scott JD (2006). Dynamic regulation of cAMP synthesis through anchored PKA–adenylyl cyclase V/VI complexes. Mol Cell 23, 925–931.

Beals CR, Clipstone NA, Ho SN, Crabtree GR (1997). Nuclear localization of NF-ATc by a calcineurin-dependent, cyclosporin-sensitive intramolecular interaction. Genes Dev 11, 824–834.

Brehm P, Eckert R (1978). Calcium entry leads to inactivation of calcium channel in *Paramecium*. Science 202, 1203–1206.

Carr DW, Hausken ZE, Fraser ID, Stofko-Hahn RE, Scott JD (1992). Association of the type II cAMP-dependent protein kinase with a human thyroid RII-anchoring protein. Cloning and characterization of the RII-binding domain. J Biol Chem 267, 13376–13382.

Catterall WA (2011). Voltage-gated calcium channels. Cold Spring Harb Perspect Biol 3, a003947.

Chen L, Glover JN, Hogan PG, Rao A, Harrison SC (1998). Structure of the DNA-binding domains from NFAT, Fos and Jun bound specifically to DNA. Nature 392, 42–48.

Coghlan VM, Perrino BA, Howard M, Langeberg LK, Hicks JB, Gallatin WM, Scott JD (1995). Association of protein kinase A and protein phosphatase 2B with a common anchoring protein. Science 267, 108–111.

Culbertson CT, Jacobson SC, Michael Ramsey J (2002). Diffusion coefficient measurements in microfluidic devices. Talanta 56, 365–373.

Dell'Acqua ML, Faux MC, Thorburn J, Thorburn A, Scott JD (1998). Membrane-targeting sequences on AKAP79 bind phosphatidylinositol-4, 5-bisphosphate. EMBO J 17, 2246–2260.

Di Biase V, Obermair GJ, Szabo Z, Altier C, Sanguesa J, Bourinet E, Flucher BE (2008). Stable membrane expression of postsynaptic CaV1.2 calcium channel clusters is independent of interactions with AKAP79/150 and PDZ proteins. J Neurosci 28, 13845–13855.

Dittmer PJ, Dell'Acqua ML, Sather WA (2014). Ca2+/calcineurin-dependent inactivation of neuronal L-type Ca2+ channels requires priming by AKAP-anchored protein kinase A. Cell Rep 7, 1410–1416.

Dolmetsch RE, Pajvani U, Fife K, Spotts JM, Greenberg ME (2001). Signaling to the nucleus by an L-type calcium channel-calmodulin complex through the MAP kinase pathway. Science 294, 333–339.

Efendiev R, Samelson BK, Nguyen BT, Phatarpekar PV, Baameur F, Scott JD, Dessauer CW (2010). AKAP79 interacts with multiple adenylyl cyclase (AC) isoforms and scaffolds AC5 and -6 to alpha-amino-3-hydroxyl-5-methyl-4-isoxazole-propionate (AMPA) receptors. J Biol Chem 285, 14450–14458.

Erickson MG, Alseikhan BA, Peterson BZ, Yue DT (2001). Preassociation of calmodulin with voltage-gated Ca(2+) channels revealed by FRET in single living cells. Neuron 31, 973–985.

Erickson MG, Liang H, Mori MX, Yue DT (2003). FRET two-hybrid mapping reveals function and location of L-type Ca2+ channel CaM preassociation. Neuron 39, 97–107.

Gao S, Wang HY, Malbon CC (2011). AKAP12 and AKAP5 form higher-order hetero-oligomers. J Mol Signal 6, 8.

Gao T, Yatani A, Dell'Acqua ML, Sako H, Green SA, Dascal N, Scott JD, Hosey MM (1997). cAMP-dependent regulation of cardiac L-type Ca2+ channels requires membrane targeting of PKA and phosphorylation of channel subunits. Neuron 19, 185–196.

Gold MG, Stengel F, Nygren PJ, Weisbrod CR, Bruce JE, Robinson CV, Barford D, Scott JD (2011). Architecture and dynamics of an A-kinase anchoring protein 79 (AKAP79) signaling complex. Proc Natl Acad Sci USA 108, 6426–6431.

Gomez LL, Alam S, Smith KE, Horne E, Dell'Acqua ML (2002). Regulation of A-kinase anchoring protein 79/150-cAMP-dependent protein kinase postsynaptic targeting by NMDA receptor activation of calcineurin and remodeling of dendritic actin. J Neurosci 22, 7027–7044.

Graef IA, Mermelstein PG, Stankunas K, Neilson JR, Deisseroth K, Tsien RW, Crabtree GR (1999). L-type calcium channels and GSK-3 regulate the activity of NF-ATc4 in hippocampal neurons. Nature 401, 703–708.

Grover LM (1998). Evidence for postsynaptic induction and expression of NMDA receptor independent LTP. J Neurophysiol 79, 1167–1182.

Grover LM, Teyler TJ (1990). Two components of long-term potentiation induced by different patterns of afferent activation. Nature 347, 477–479.

Hall DD, Davare MA, Shi M, Allen ML, Weisenhaus M, McKnight GS, Hell JW (2007). Critical role of cAMP-dependent protein kinase anchoring to the L-type calcium channel Cav1.2 via A-kinase anchor protein 150 in neurons. Biochemistry 46, 1635–1646.

Hoshi N, Langeberg LK, Scott JD (2005). Distinct enzyme combinations in AKAP signalling complexes permit functional diversity. Nat Cell Biol 7, 1066–1073.

Klauck TM, Faux MC, Labudda K, Langeberg LK, Jaken S, Scott JD (1996). Coordination of three signaling enzymes by AKAP79, a mammalian scaffold protein. Science 271, 1589–1592.

Kouzarides T, Ziff E (1988). The role of the leucine zipper in the fos–jun interaction. Nature 336, 646–651.

Kremers GJ, Goedhart J, van den Heuvel DJ, Gerritsen HC, Gadella TW (2007). Improved green and blue fluorescent proteins for expression in bacteria and mammalian cells. Biochemistry 46, 3775–3783.

Landschulz WH, Johnson PF, McKnight SL (1988). The leucine zipper: a hypothetical structure common to a new class of DNA binding proteins. Science 240, 1759–1764.

Li H, Pink MD, Murphy JG, Stein A, Dell'Acqua ML, Hogan PG (2012). Balanced interactions of calcineurin with AKAP79 regulate Ca2+–calcineurin–NFAT signaling. Nat Struct Mol Biol 19, 337–345.

Li J, Negro A, Lopez J, Bauman AL, Henson E, Dodge-Kafka K, Kapiloff MS (2010). The mAKAPbeta scaffold regulates cardiac myocyte hypertrophy via recruitment of activated calcineurin. J Mol Cell Cardiol 48, 387–394.

Ma H, Cohen S, Li BX, Tsien RW (2013). Exploring the dominant role of Cav1 channels in signalling to the nucleus. Bioscience Rep 33, 97–101.

Magde D, Elson E, Webb WW (1972). Thermodynamic fluctuations in a reacting system—measurement by fluorescence correlation spectroscopy. Phys Rev Lett 29, 705.

Malenka RC, Bear MF (2004). LTP and LTD: an embarrassment of riches. Neuron 44, 5–21.

Moosmang S, Haider N, Klugbauer N, Adelsberger H, Langwieser N, Muller J, Stiess M, Marais E, Schulla V, Lacinova L, *et al*. (2005). Role of hippocampal Cav1.2 Ca2+ channels in NMDA receptor-independent synaptic plasticity and spatial memory. J Neurosci 25, 9883–9892.

Morgan SL, Teyler TJ (1999). VDCCs and NMDARs underlie two forms of LTP in CA1 hippocampus in vivo. J Neurophysiol 82, 736–740.

Müller P, Schwille P, Weidemann T (2014). PyCorrFit—generic data evaluation for fluorescence correlation spectroscopy. Bioinformatics 30, 2532–2533.

Murphy JG, Sanderson JL, Gorski JA, Scott JD, Catterall WA, Sather WA, Dell'Acqua ML (2014). AKAP-anchored PKA maintains neuronal L-type calcium channel activity and NFAT transcriptional signaling. Cell Rep 7, 1577–1588.

Murphy TH, Worley PF, Baraban JM (1991). L-type voltage-sensitive calcium channels mediate synaptic activation of immediate early genes. Neuron 7, 625–635.

Oliveria SF, Dell'Acqua ML, Sather WA (2007). AKAP79/150 anchoring of calcineurin controls neuronal L-type Ca2+ channel activity and nuclear signaling. Neuron 55, 261–275.

Oliveria SF, Dittmer PJ, Youn DH, Dell'Acqua ML, Sather WA (2012). Localized calcineurin confers Ca2+-dependent inactivation on neuronal L-type Ca2+ channels. J Neurosci 32, 15328–15337.

Oliveria SF, Gomez LL, Dell'Acqua ML (2003). Imaging kinase–AKAP79–phosphatase scaffold complexes at the plasma membrane in living cells using FRET microscopy. J Cell Biol 160, 101–112.

Ortner NJ, Striessnig J (2016). L-type calcium channels as drug targets in CNS disorders. Channels (Austin) 10, 7–13.

Peterson BZ, DeMaria CD, Adelman JP, Yue DT (1999). Calmodulin is the Ca^{2+} sensor for Ca^{2+}-dependent inactivation of L-type calcium channels. Neuron 22, 549–558.

Phair RD, Misteli T (2000). High mobility of proteins in the mammalian cell nucleus. Nature 404, 604–609.

Sassone-Corsi P, Ransone LJ, Lamph WW, Verma IM (1988). Direct interaction between fos and jun nuclear oncoproteins: role of the "leucine zipper" domain. Nature 336, 692–695.

Smith KE, Gibson ES, Dell'Acqua ML (2006). cAMP-dependent protein kinase postsynaptic localization regulated by NMDA receptor activation through translocation of an A-kinase anchoring protein scaffold protein. J Neurosci 26, 2391–2402.

Sochivko D, Chen J, Becker A, Beck H (2003). Blocker-resistant Ca2+ currents in rat CA1 hippocampal pyramidal neurons. Neuroscience 116, 629–638.

Tavalin SJ (2008). AKAP79 selectively enhances protein kinase C regulation of GluR1 at a Ca2+-calmodulin-dependent protein kinase II/protein kinase C site. J Biol Chem 283, 11445–11452.

Wild AR, Dell'Acqua ML (2018). Potential for therapeutic targeting of AKAP signaling complexes in nervous system disorders. Pharmacol Ther 185, 99–121.

Wild AR, Sinnen BL, Dittmer PJ, Kennedy MJ, Sather WA, Dell'Acqua ML (2019). Synapse-to-nucleus communication through NFAT is mediated by L-type Ca(2+) channel Ca(2+) spike propagation to the soma. Cell Rep 26, 3537–3550 e3534.

Woolfrey KM, Dell'Acqua ML (2015). Coordination of protein phosphorylation and dephosphorylation in synaptic plasticity. J Biol Chem 290, 28604–28612.